Electronic Supporting Information for

X-ray Irradiation-Induced Luminescent Silver Clusters Formation In Nanoporous Matrices

Eduardo Coutino-Gonzalez,[a] Didier Grandjean,[b] Maarten B.J. Roeffaers,[c] Kristina Kvashnina,[d] Bjorn Dieu,[a] Eduard Fron,[a] Gert De Cremer,[c,e] Peter Lievens,[b] Bert Sels,[c,*] and Johan Hofkens[a,*]

[a]Department of Chemistry, KU Leuven, Celestijnenlaan 200F, B-3001 Leuven, Belgium

[b]Department of Physics and Astronomy, Laboratory of Solid State Physics and Magnetism, KU Leuven, Celestijnenlaan 200D, B-3001 Leuven, Belgium

[c]Department of Microbial and Molecular Systems, Centre for Surface Chemistry and Catalysis, KU Leuven, Kasteelpark Arenberg 23, B-3001 Leuven, Belgium

[d]European Synchrotron Radiation Facility (ESRF), 6 Rue Jules Horowitz, BP220, 38043 Grenoble Cedex 9, France

[e]Current address: DSM Ahead, Urmonderbaan 22, 6167-RD Geleen, The Netherlands

*Corresponding author: johan.hofkens@chem.kuleuven.be, bert.sels@biw.kuleuven.be

S1. Scanning electron microscope (SEM) pictures of LTA and FAU topologies.

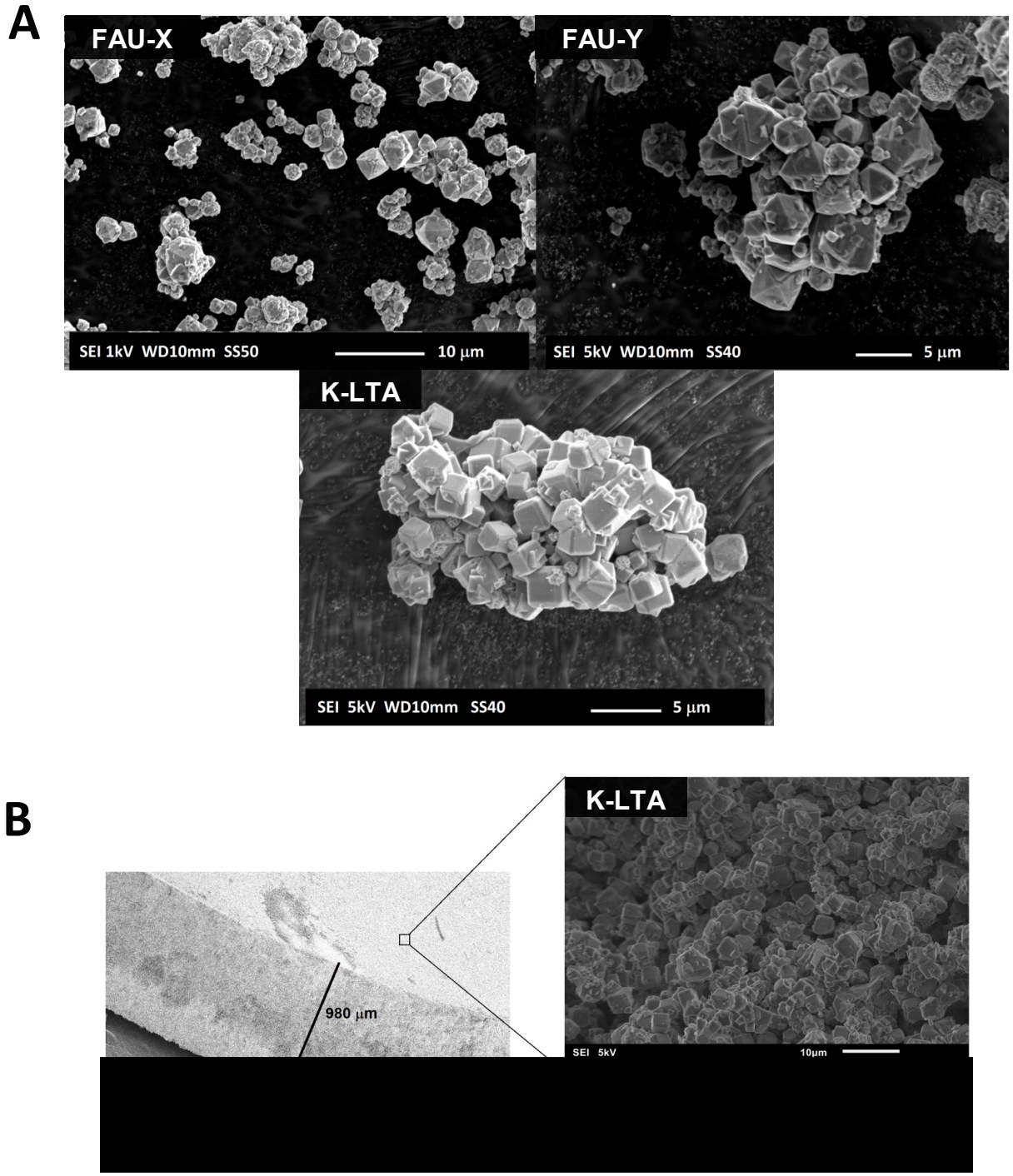

Figure S1. SEM images of the starting materials used in this study (FAU-X, FAU-Y and LTA). A. Images of the loose powders. B. Cross-section of a pellet made by K-LTA. The images were recorded on a JEOL-6010LV SEM using non-coated samples.

S2. Zeolites chemical composition and silver loadings. In table 1 the chemical composition of the three zeolites employed in this study is shown. They possess different silicon to aluminium ratios (Si/Al); therefore the amount of silver ions that can be loaded via cation exchange in the framework of the zeolite is different for each topology. LTA (in its K form) has a Si/Al ratio of 1 whereas FAU-X and FAU-Y have a Si/Al of 1.2 and 2.7 respectively, this means that in LTA more counter-balancing cations can be accommodated within the framework. In the present report we used the following configurations for the different samples;

- $|Ag^{+}_{3}K^{+}_{9}|\ [Al_{12}Si_{12}O_{48}]\ |H_2O|_{27}$, referred as Ag_3K_9-LTA
- $|Ag^{+}_{9}K^{+}_{3}|\ [Al_{12}Si_{12}O_{48}]\ |H_2O|_{27}$, referred as Ag_9K_3-LTA
- $|Ag^{+}_{6}Na^{+}_{5}|\ [Al_{11}Si_{13}O_{48}]\ |H_2O|_{27.5}$, referred as Ag_6Na_5-FAU-X
- $|Ag^{+}_{3}Na^{+}_{3.5}|\ [Al_{6.5}Si_{17.5}O_{48}]\ |H_2O|_{27.5}$, referred as $Ag_3Na_{3.5}$-FAU-Y

Table S1. Chemical composition of a unit cell of the different zeolites used in this study.

Zeolite	Structural formula
K-LTA	$\|K^{+}_{12}\|\ [Al_{12}Si_{12}O_{48}]\ \|H_2O\|_{27}$
FAU-X	$\|Na^{+}_{11}\|\ [Al_{11}Si_{13}O_{48}]\ \|H_2O\|_{27.5}$
FAU-Y	$\|Na^{+}_{6.5}\|\ [Al_{6.5}Si_{17.5}O_{48}]\ \|H_2O\|_{27.5}$

The structural formulas were obtained after normalization of the total amount of T atoms in the unit cell to 24.

S3. Emission and excitation of the X-ray activated and heat-treated silver containing zeolites. The silver-containing X-ray activated pellets and heat-treated samples were placed and sealed between 2 quartz plates. Emission spectra were recorded at different excitation wavelengths from 260 to 680 nm with 5 nm intervals, using a Quanta Master 60 fluorimeter (PTI). For every excitation wavelength, the emission was collected starting 10 nm above the excitation wavelength

and ending at 800 nm using 10 nm steps. The signal above 410 nm was measured using a 400 nm long pass glass filter to avoid interference from second-order excitation peaks, the measured intensities were corrected for the transmittance of the long pass filter. The emission was collected in "front face mode" through the quartz plates and sent to a PMT for detection. From the separate emission spectra at varying excitation wavelengths, the two dimensional excitation-emission matrices were constructed, the raw data was corrected for background and noise and interpolated to a resolution of 1 nm x 1 nm. For comparison, the 2-dimensional excitation-emission plots of the analogous heat-treated samples were also recorded.

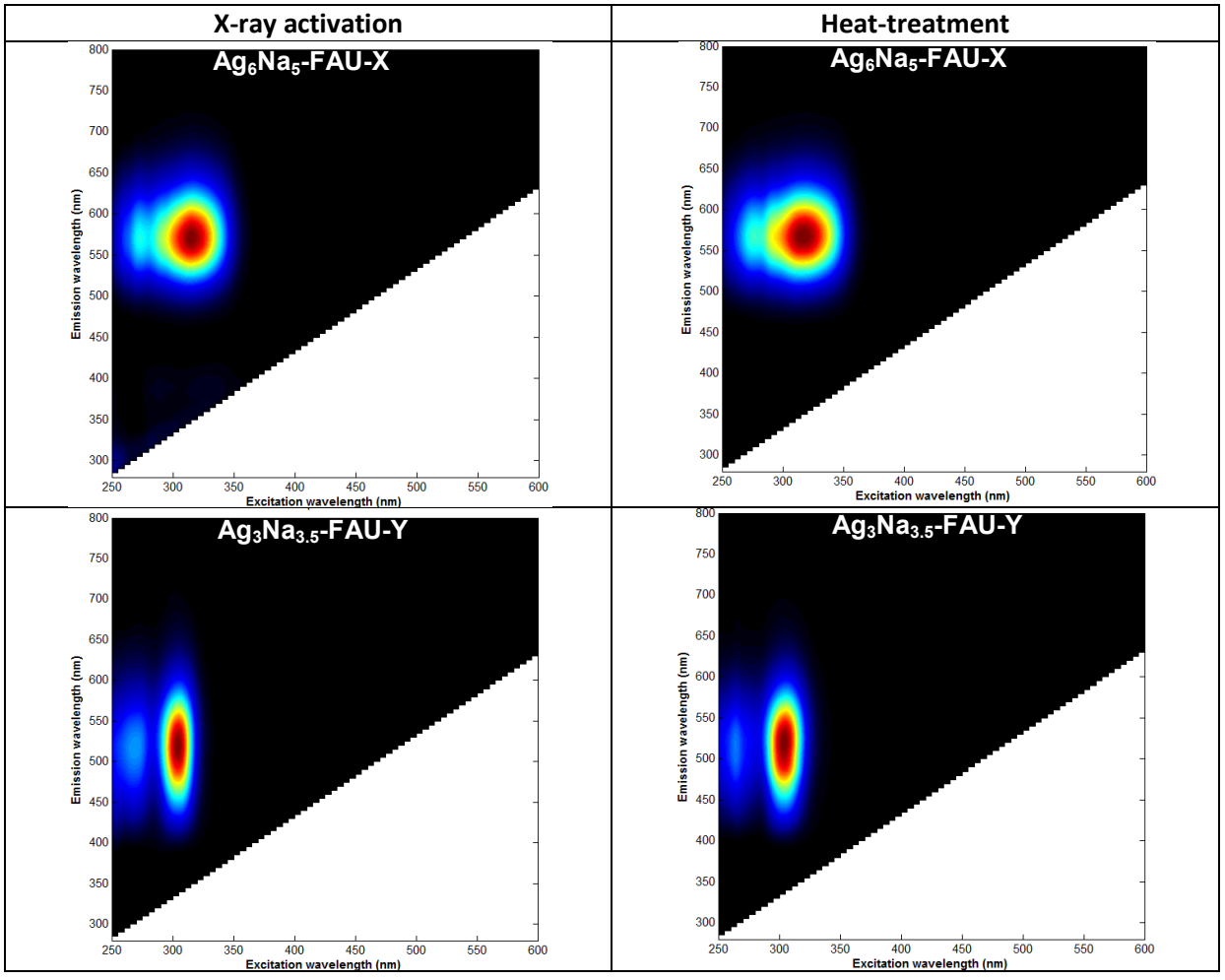

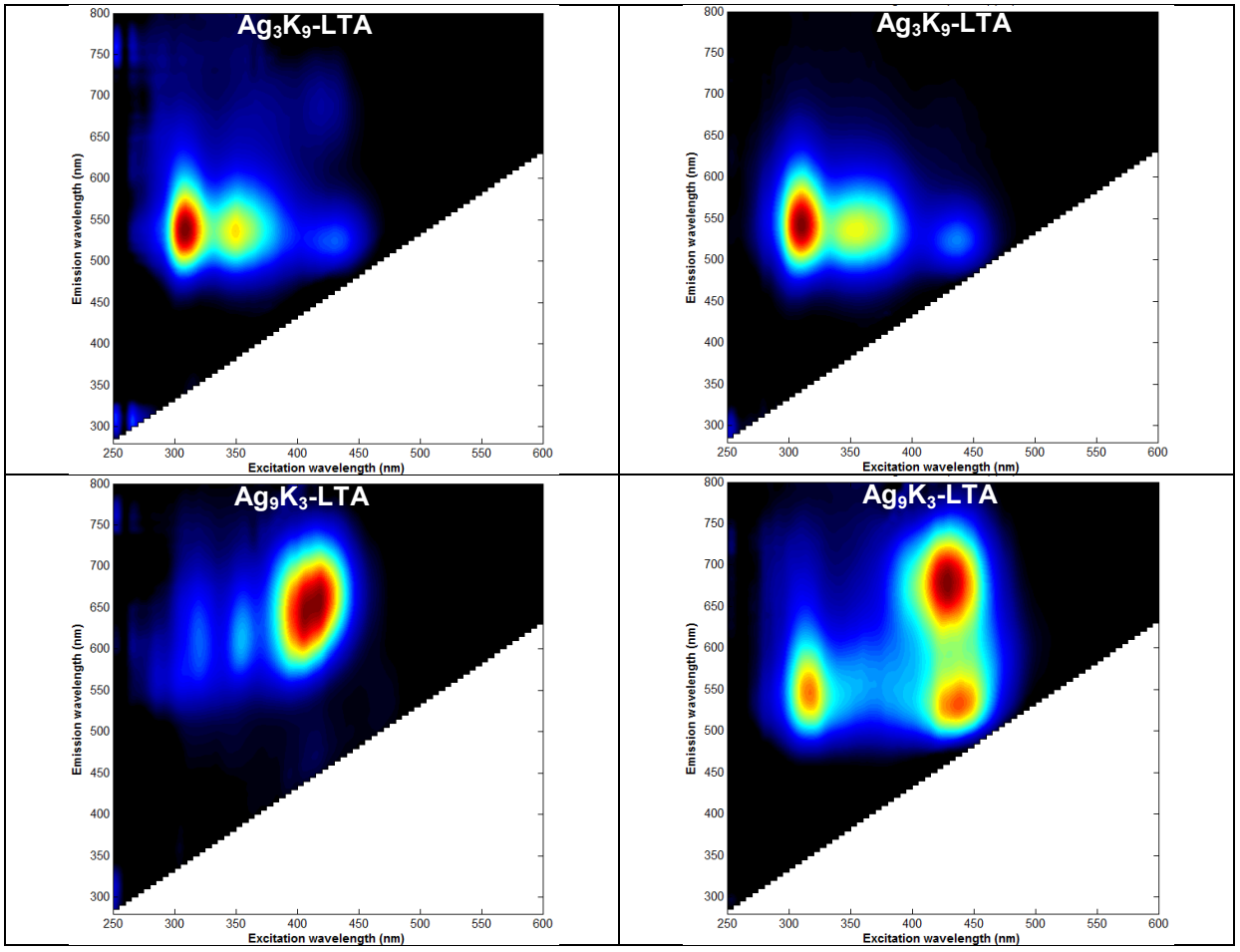

Figure S2. Two-dimensional excitation-emission plots of the X-ray activated (left) and heat-treated (right) silver loaded zeolites, Ag_6Na_5-FAU-X, $Ag_3Na_{3.5}$-FAU-Y, Ag_3K_9-LTA and Ag_9K_3-LTA.

No significant differences between most of the X-ray activated and heat-treated silver loaded zeolites were found. Nevertheless, for sample Ag_9K_3-LTA a more specific production of the red emitting species was found in the X-ray activated sample, whereas for the analogous heat-treated sample a mixture of green and red emitting species was observed. In the excitation-emission plots of the heat-treated and X-ray irradiated samples, the presence of multiple peaks can be observed. This can be associated to differences in size, shape, charge, and interactions with the environment

of the luminescent silver clusters.[1] In Ag_3K_9-LTA (heat-treated and X-ray irradiated) an emission maximum at ~540 nm when excited at three different excitation wavelengths (310, 340, and 440 nm) was observed. In heat-treated Ag_9K_3-LTA two emission maxima where found at 540 and 700 nm when excited at 310 and 440 nm respectively, whereas in X-ray activated Ag_9K_3-LTA a single emission maximum can be observed at ~670 nm under 410 nm excitation.

There is a wide agreement on the preferential formation and stabilization of Ag_{3-4}^{n+} and Ag_6^{n+} clusters in the sodalite cages of heat-treated silver exchanged LTA zeolites. Ag_{3-4}^{n+} clusters, responsible for the green emission, were preferentially observed when low silver loadings were used.[2] The different excitation wavelengths encountered in Ag_3K_9-LTA, could be associated with different environments that Ag_{3-4}^{n+} clusters experienced. In high silver loaded samples (Ag_9K_3-LTA), the presence of two emission maxima (540 and 700 nm) could be associated with the presence of two different emitting clusters, Ag_{3-4}^{n+} and Ag_6^{n+}. It has been proposed that hexa-atomic silver cluster could be formed by the interaction of two Ag_{3-4}^{n+} clusters.[2,3] The presence of both emitting species in the calcined sample reveals the low specificity and selectivity of the heat-treatment, compared to the X-ray activation procedure in which, for the same sample, a single emission maximum at ~670 nm was observed when excited at 410 nm.

While in silver exchanged LTA zeolites both clusters (Ag_{3-4}^{n+} and Ag_6^{n+}) have been observed, there is not clear evidence in literature for the presence of a hexa-atomic silver clusters in FAU zeolites. It has rather been proposed that, after formation of Ag_{3-4}^{n+} clusters in the sodalite cages of silver exchanged FAU zeolites, further clustering is inhibited.[3-5]

The excitation-emission plots of the non-activated samples were recorded as references. Fig. S3 shows the obtained results for Ag_3K_9-LTA and Ag_9K_3-LTA samples, no emission was observed. A similar behavior was found for Ag_6Na_5-FAU-X and $Ag_3Na_{3.5}$-FAU-Y non-activated samples.

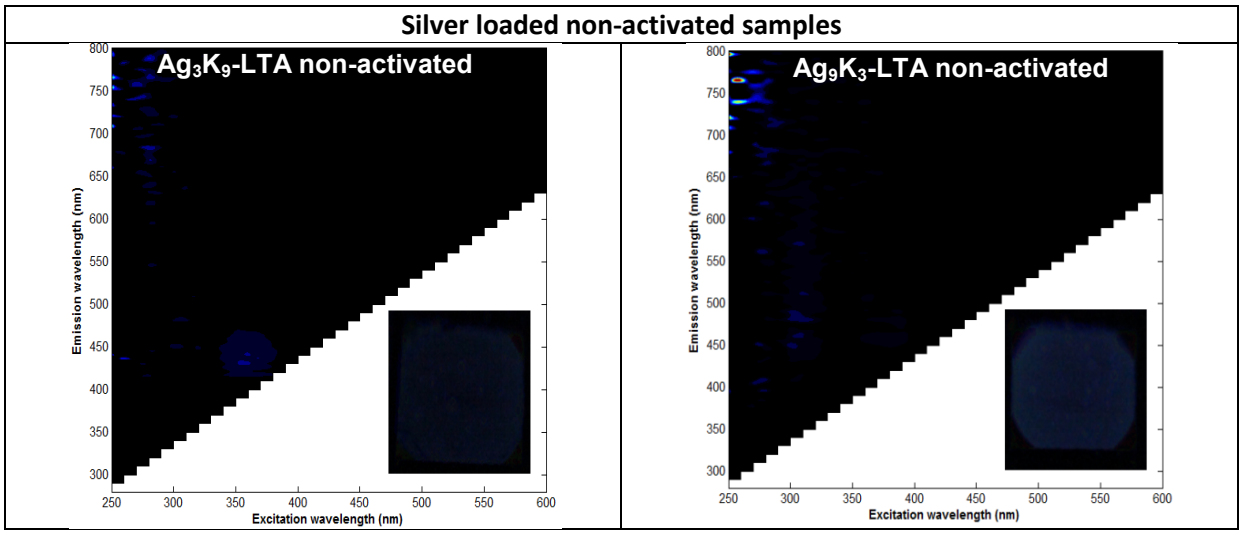

Figure S3. 2D excitation-emission plots of the non-activated Ag_3K_9-LTA and Ag_9K_3-LTA; inset: pictures of the samples taken under 366 nm illumination.

The distribution of the luminescence through the X-ray activated silver exchanged zeolite crystals was found to be homogeneous as demonstrated by the series of optical confocal sections throughout X-ray irradiated Ag_3K_9-LTA crystals collected with a confocal microscope (Fluoview 1000 Olympus, 405 nm excitation) presented in Figure S4, indicating that the luminescent silver clusters are distributed along the zeolite crystals homogenously.

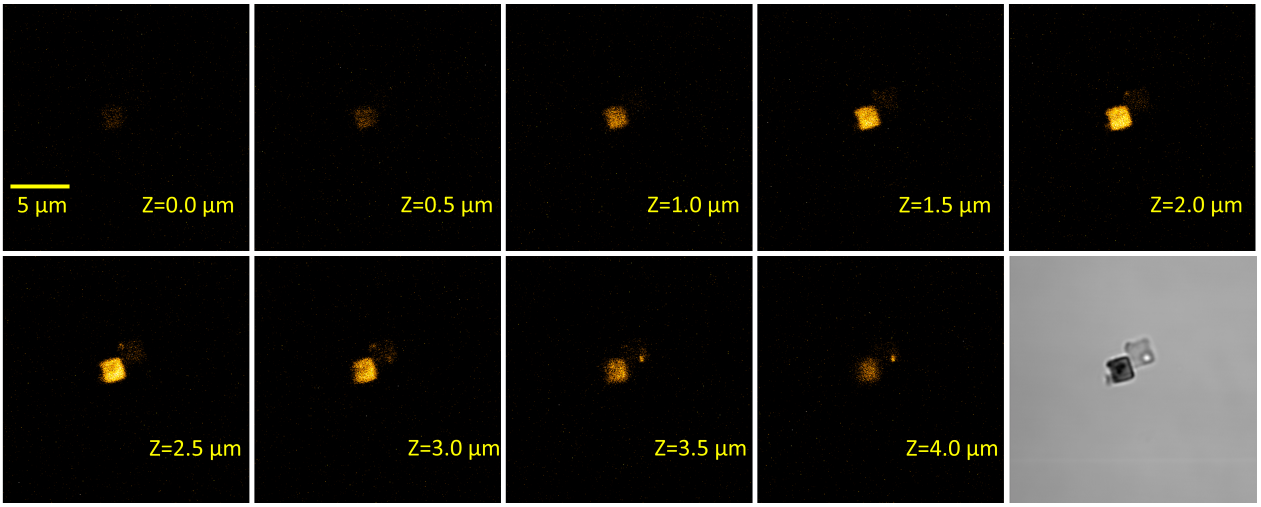

Figure S4. Series of optical confocal sections through both, an X-ray activated and a non-activated Ag_3K_9-LTA crystal. The right down panel shows the transmission image in which two different crystals are observed, however, only the crystal submitted to X-ray irradiation (left) is clearly seen on the false color fluorescence images of the crystals.

Finally, we performed SEM measurements on the X-ray activated samples to investigate the possible formation of larger silver nanoparticles on the surface of the zeolite crystals, however as it is mentioned in several reports,[6,7] silver exchanged zeolites are very sensitive to highly energetic probe beams, such as electrons and X-rays. In a recent study,[8] the formation of silver clusters and nanoparticles by electron beam irradiation of silver exchanged LTA and FAU zeolites was reported, the disruption of the chemical bonds (due to the electron beam) within the zeolite framework which favored the coalescence of silver atoms/clusters to form a larger nanoparticle phase, was attributed as a possible formation mechanism. To investigate the effect of the electron beam on the X-ray activated samples we recorded a series of SEM images of the same region with different exposure times. At time zero the presence of larger nanoparticles were not observed on the surface of the probed zeolite crystals (Fig. S5-A). However, when the same region was exposed for a certain time to the electron beam, the emergence of silver nanoparticles on the surface of certain zeolite crystals was observed (Fig. S5-B).

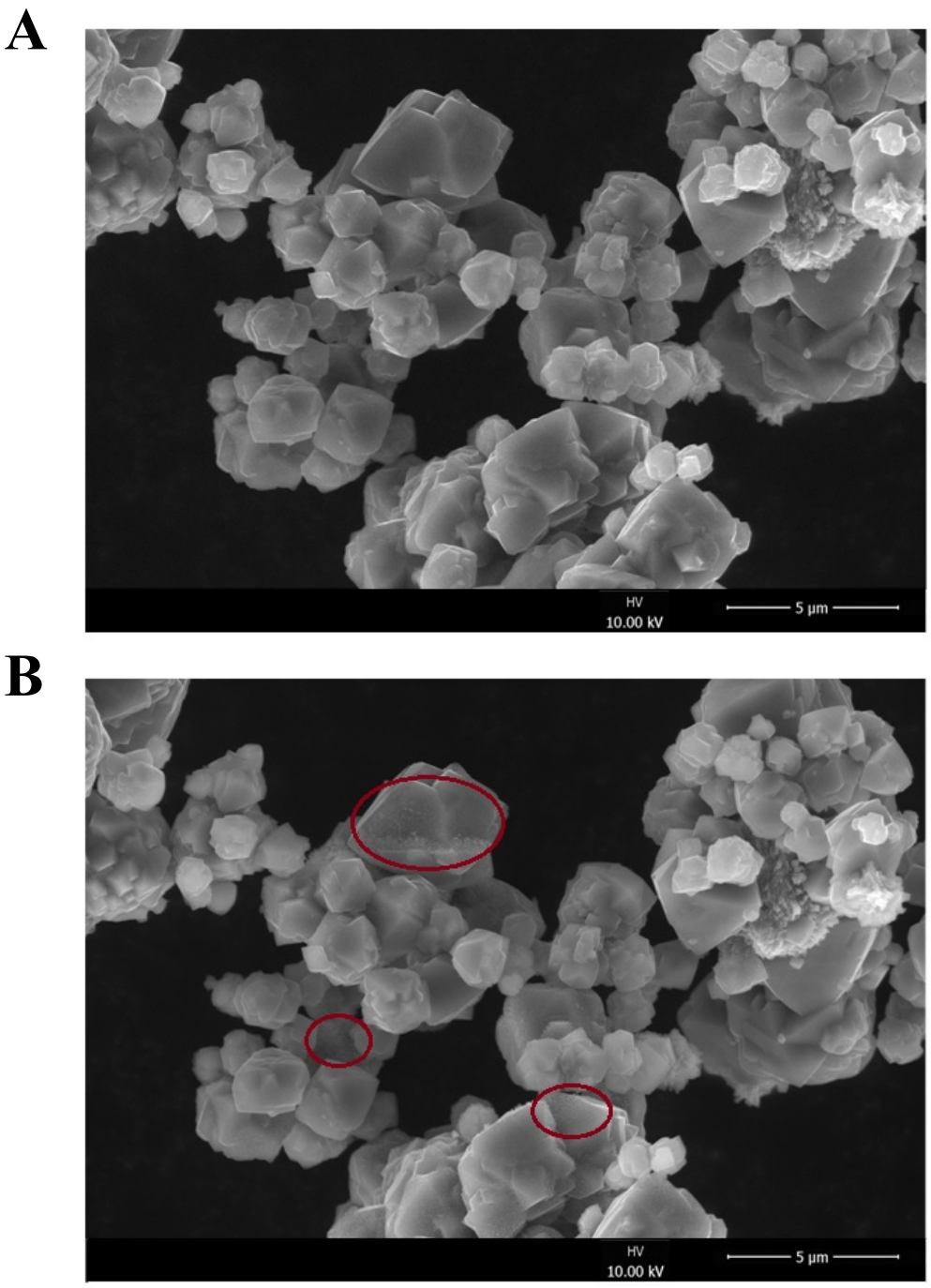

Figure S5. SEM images of the X-ray irradiated Ag_6Na_5-FAU-X sample, at time zero (A) and after 2 minutes of electron beam exposure (B). The red circles indicate the regions where larger silver nanoparticles were observed. The exposure time to induce the production of silver nanoparticles on the surface of X-ray irradiated silver exchanged zeolites, ranged between 1 and 5 minutes depending on the zeolite topology and the silver content, high silver loaded LTA samples were affected faster compared to silver exchanged FAU-Y samples.

S4. Diffuse reflectance spectroscopy (DRS) and comparison between $Ag_3Na_{3.5}$-FAU-Y in dehydrated and hydrated forms. An UV-Vis-NIR Lambda 950 Perkin Elmer spectrophotometer equipped with a 150 mm diameter integrating sphere (coated with Spectralon) was used to record the DRS spectra. The samples were placed in a Teflon sample holder and covered with a quartz plate for measurements.

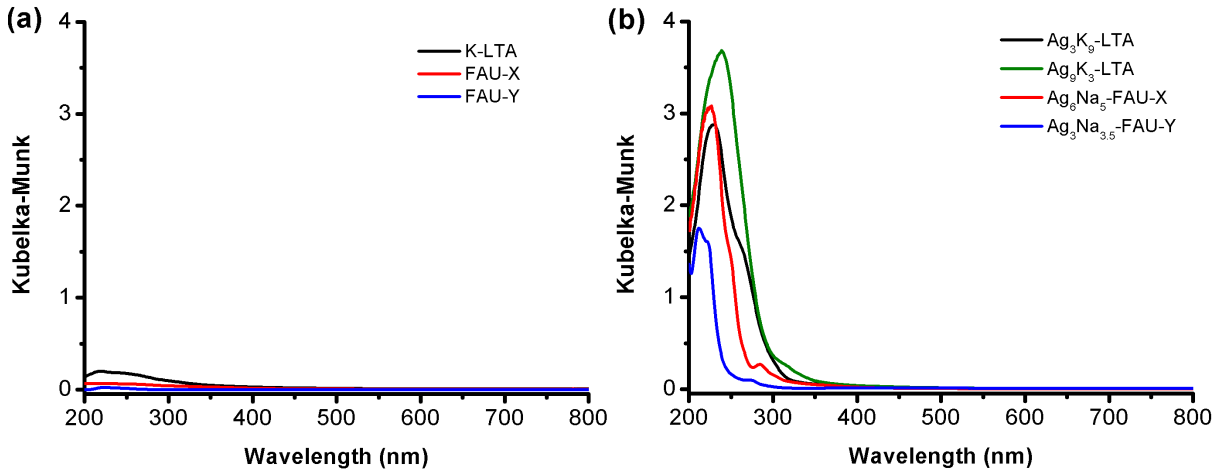

Figure S6. DRS spectra of (a) pure non-exchanged zeolites and (b) silver loaded non-activated zeolites.

DRS spectra of pure non-exchanged and silver exchanged non-activated zeolites are shown in Fig. S6. No representative signals corresponding to absorbing species in the DRS spectra of non-exchanged zeolites were found, whereas in the silver loaded non-activated zeolites, strong signals appeared in the UV region. Such signals have been previously associated to isolated silver ions located at specific sites within the zeolite framework in silver exchanged LTA and FAU zeolites.[9] DRS spectra of the X-ray irradiated silver loaded zeolites showed the appearance of new absorbing bands that were not present in non-exchanged zeolites nor in silver loaded non-activated samples (Fig. S7-A). Finally, we carried out a detailed analysis and comparison of the DRS spectra of X-ray

irradiated and heat-treated $Ag_3Na_{3.5}$-FAU-Y samples that present a strong influence of hydration level on their emission and absorption properties.

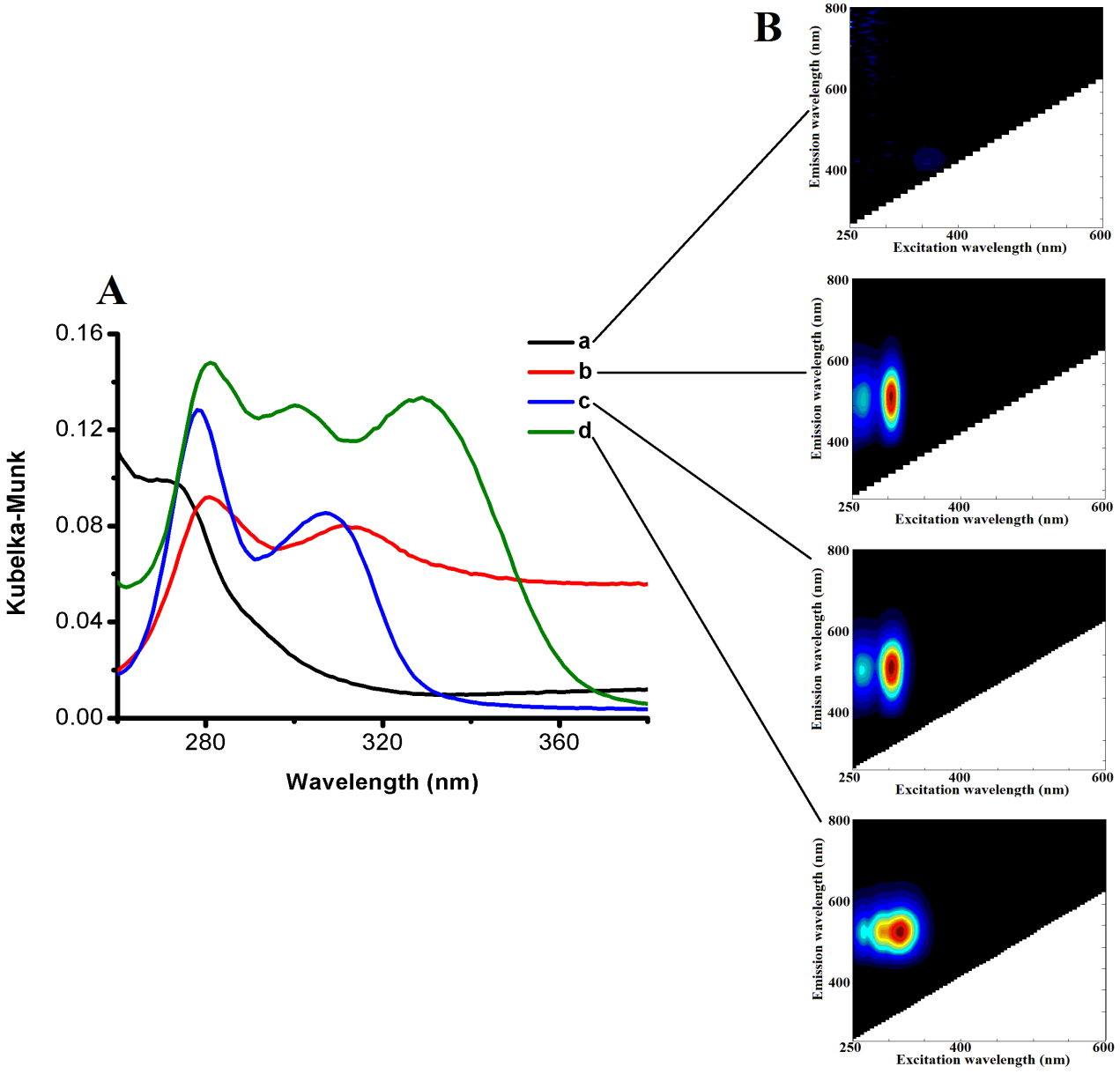

Fig. S7. A) DRS spectra and B) two-dimensional excitation-emission plots of $Ag_3Na_{3.5}$-FAU-Y non-activated (a), X-ray irradiated (b), heat-treated hydrated, (c) and heat-treated dehydrated (d). The DRS spectra of the irradiated pellets were recorded using a mask to reduce the region of analysis, due to this modification and to the non uniform irradiated surface area of the pellets, a quantitative comparison cannot be performed.

In heat-treated dehydrated $Ag_3Na_{3.5}$-FAU-Y three absorption bands (280, 300 and 330 nm) are observed in the DRS spectrum (Fig. S7-A), these three bands can be correlated to the three excitation wavelengths found in the two-dimensional excitation-emission plot that resulted in an emission maxima at 530 nm. For $Ag_3Na_{3.5}$-FAU-Y heat-treated hydrated sample, two absorption bands were found in the DRS spectrum at 280 and 310 nm, analysis of the 2D excitation-emission plot (Fig. S7-B) revealed the presence of two excitation wavelengths (270 and 310 nm) that resulted in emission at 520 nm. X-ray irradiated $Ag_3Na_{3.5}$-FAU-Y display a similar behavior as the heat-treated hydrated sample, the presence of two absorption bands at 280 and 310 with the respective excitation wavelengths at 270 and 310 resulting in emission at 520 nm, indicates a high similitude between the X-ray irradiated and the heat-treated hydrated samples. The X-ray irradiation was performed on the surface of a pelletized sample at ambient conditions, it is reasonable to assume that the created luminescent samples stay in their hydrated form. The DRS and two-dimensional excitation-emission measurements of dehydrated samples were performed right after the heat-treatment, whereas the measurements on hydrated samples were performed on samples exposed to the ambient overnight after the heat-treatment. No absorption bands nor excitation-emission peaks were found in the non-activated $Ag_3Na_{3.5}$-FAU-Y sample, within the region explored.

S5. X-ray absorption near-edge structure (XANES) measurements and X-ray activation of silver clusters embedded in zeolite matrices.

X-ray irradiation of the different samples was performed at beamline ID26[10] of the European Synchrotron Radiation Facility (ESRF) in Grenoble operating under uniform filling mode. The electron energy was 6.0 GeV, with a ring current ranging from 170 to 200 mA. The first harmonic

of one u40 and two u35 undulators was used and the rejection of higher harmonics was achieved by three Si mirrors at an angle of 3.5 mrad relative to the incident beam. For each irradiation time the incident energy selected using the <111> reflection from a double Si crystal monochromator was scanned from 3510-3600 eV around the Ag L_2 edge (3524 eV) calibrated with a metal silver foil. X-ray absorption near-edge structure (XANES) spectra were measured in high-energy-resolution fluorescence detection (HERFD) mode using a X-ray emission spectrometer.[11] The sample, analyzer crystal and photon detector (silicon drift diode) were arranged in a vertical Rowland geometry. The Ag HERFD spectra at the L_2 edge were obtained by recording the maximum intensity of the Ag $L\beta_1$ emission line (~3150.5 eV) as a function of the incident energy. The emission energy was selected using the <440> reflection of four spherically bent Ge crystal analyzers (with 1m bending radius) aligned at 80° Bragg angle. The paths of the incident and emitted X-rays through air were minimized in order to avoid losses in intensity due to absorption. The intensity was normalised to the incident flux. A combined (incident convoluted with emitted) energy resolution of 0.4 eV was obtained as determined by measuring the full width at half maximum (FWHM) of the elastic peak. The present data is not corrected for self-absorption effects. The analysis shown in this work is based on comparison of the energy position of the main transitions at the Ag L_2 edge which is only little affected by self-absorption effects. The XANES spectra of the luminescent material was measured with 10 s time resolution on 100 different locations and averaged. XANES of the non-luminescent black region was measured once with a time resolution of 4 min following a 12 min X-ray illumination. The spectra were normalized at 3554.0 eV, 30 eV above the Ag metal edge at 3524 eV.

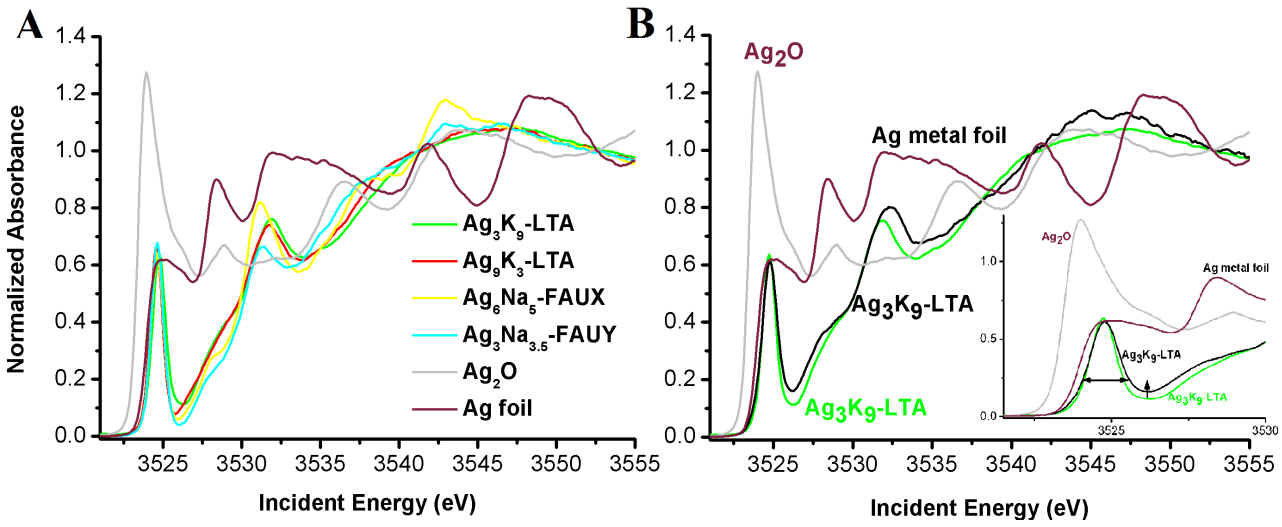

Figure S8. A) Ag L_2 edge HERFD XANES of Ag_3K_9-LTA, Ag_9K_3-LTA, Ag_6Na_5-FAUX and $Ag_3Na_{3.5}$-FAU-Y. B) Ag L_2 edge HERFD XANES of luminescent (green line) and non-luminescent (black line) X-ray beam modified Ag_3K_9-LTA; inset: zoomed area.

HERFD detection mode improves the resolution of the X-ray Absorption spectra by taking advantage of the decreased final state core-hole lifetime broadening of the specific fluorescence channel detected by a secondary energy-selective spectrometer.[12] XANES provides information on the local electronic and geometric structure of the silver species. For most metals the intensity of the white line of a L_2 edge XANES spectrum generally reveals the unfilled d band and is sensitive to the metal oxidation state and the presence of adsorbates on the surface.[13] Following the dipole selection rules at the Ag L_2 edge, electrons are excited from $2p_{1/2}$ core level into unoccupied states of *s* and *d* character ($L = \pm 1$). However, Ag^0 and Ag^+ have a $4d^{10}$ configuration and no white line is expected due to the fully occupied state. The distinctive peak of the white line appearing at the Ag L_2 X-ray absorption edge is formally assign to 2p to 5s excitations. The 2p-5s excitations in general are very weak but the intensity is borrowed from 4d level through the 5s-4d hybridization.[14] A detailed interpretation of the HERFD-XANES spectra recorded during the formation and the subsequent degradation of the luminescent Ag species is underway using FEFF

and DFT techniques.

A 13 mm diameter pressed pellet (1.5 tons) of each sample was placed at a scattering angle of 45 degrees to the incident beam. Two pairs of slits 200 μm x 1000 μm (vertical x horizontal size) installed at a distance of 1m before the sample produced a rectangular X-ray beam size of 150 μm x 300 μm (vertical x horizontal) on the sample. However, indirect activation, by scattered X-rays, of the surrounding irradiated area was observed. Irradiation patterns on each sample were created using an automated program combining constant irradiation time at a fixed position followed by a sample translation step. Each irradiated spot at the surface of the pressed pellet, corresponding to an equal X-ray illumination time (10sec, 50 sec or 60 seconds according to the sample), was separated by a distance of 300 and 1500 microns in the vertical and horizontal direction respectively. The total irradiation received by the sample on each individual spot was measured by integrating the incoming flux I_0 measured by a silicon drift diode over the irradiation time.

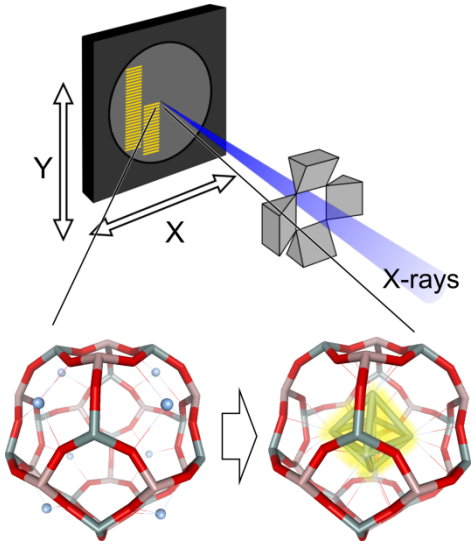

Figure S9. Schematic illustration of the irradiation strategy employed in this study. A sodalite cage (structural motive present in LTA and FAU topologies) is included for clarity, the presence of silver ions and clusters is shown schematically; however, they do not represent the real state of the silver ions and clusters in zeolite cavities. An automated translation stage was used to move the sample along the X and Y axis. Irradiation parameters can be found in Table S2.

A precise calibration run with five beam spots corresponding to incremented exposure times of 1, 2, 10, 60 and 120s was carried out for each sample before performing the automated irradiation of the whole surface (white arrows in Fig. S10). A prolonged beam exposure led systematically to the darkening of the spot (center of the luminescence pattern indicated by a red arrow in Fig. S10), likely corresponding to the transformation of silver ions and clusters into a nanostructured silver oxide phase. This is probably associated with significant X-ray beam damage of the zeolite framework itself. For each sample an optimal exposure time corresponding to a maximum of the luminescence intensity of the irradiated area, visualized under UV illumination, was determined. Selected exposure times ranging from 10 to 60s (for each irradiated spot) reflect slight discrepancies in formation mechanisms and stability of the samples.

Table S2. Irradiation parameters used for the different activated samples.

Sample	Average energy (eV)	Irradiation time (s) per spot	Average Irradiation (counts/point)	Average photon (photon/point)[a]	Total irradiation (photons)	Total irradiation (joules)[b]	Total irradiation[c] J/g	X-ray beam dose J/m^2
Ag_3K_9-LTA	3529.18	10	95950.28	6.57E+10	9.53E+12	0.005392	7.95E+01	7.19E+04
Ag_9K_3-LTA	3529.16	50	546645.1	3.74E+11	5.20E+13	0.029446	4.34E+02	3.93E+05
Ag_6Na_5-FAU-X	3529.18	10	98222.1	6.73E+10	9.76E+12	0.005519	8.14E+01	7.36E+04
$Ag_{3.5}Na_3$-FAU-Y	3529.18	60	679718.6	4.65E+11	6.47E+13	0.036614	5.40E+02	4.88E+05

[a]1 count = 685358.25 photons, [b]photons*average energy in J, 1 eV = 1.6021764E-19 J [c]irradiated surface = 7.50E-08 m^2, surface pellet = 1.32733E-04 m^2, mass pellet = 1.20E-01 g, D = 900 g/m^2, irradiated mass = 6.79E-05 g.

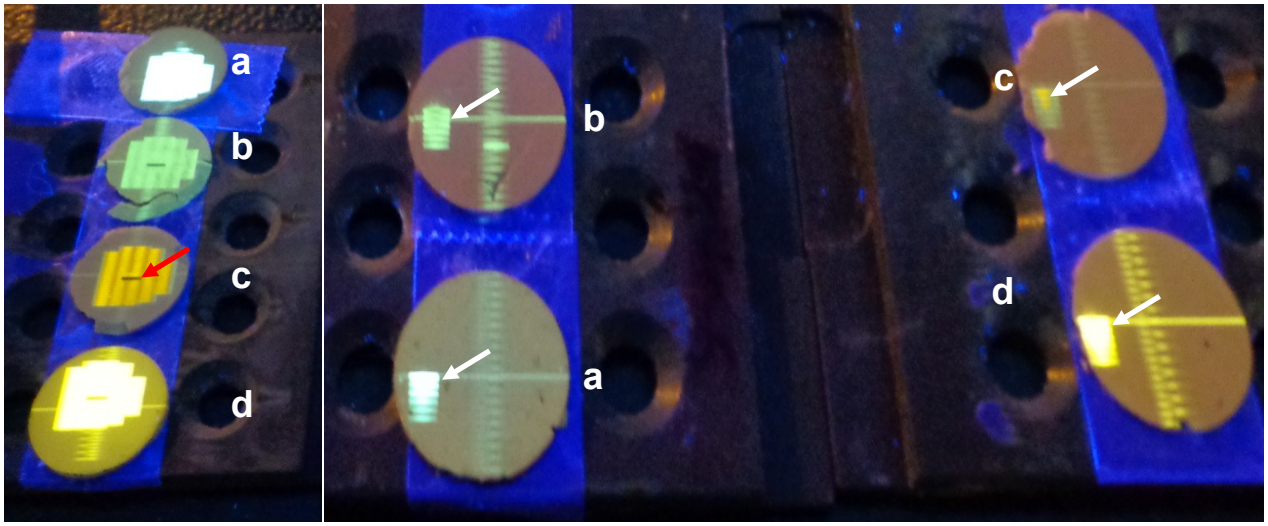

Figure S10. X-ray irradiated silver zeolite pellets in which an activation scale based on the exposure time is indicated by white arrows. a. $Ag_{3.5}Na_3$-FAU-Y, b. Ag_3K_9-LTA, c. Ag_9K_3-LTA, d. Ag_6Na_5-FAU-X.

S6. Lifetime measurements on the nanosecond time scale. The fluorescence decay times were determined by time-correlated single photon counting (TCSPC) measurements, the setup has been described in detail previously.[15] Briefly, the frequency-doubled output (375 nm, 8.18 MHz, 2 ps

FWHM) of a mode-locked Ti:sapphire laser (Tsunami, Spectra Physics) was used as excitation source. The linearly polarized excitation light was rotated to a vertical direction by the use of a Berek compensator (New Focus) in combination with a polarization filter and directed onto the sample. The sample consisting of a X-ray activated silver containing zeolite pellet sealed between two quartz plates, was mounted at an angle of 55° with respect to the incident light. The emission was collected under 90° with respect to the incident light and guided through a polarization filter that was set at the magic angle (54.7°) with respect to the polarization of the excitation beam. The fluorescence was spectrally resolved by a monochromator (Sciencetech 9030, 6-mm bandwidth), and detected by a microchannel plate photomultiplier tube (MCP-PMT, R3809U, Hamamatsu). A time-correlated single photon timing PC module (SPC 830, Becker & Hickl) was used to obtain the fluorescence decay histogram in 4096 channels. The decays were recorded with 10000 counts in the peak channel, in time windows of 25 ns corresponding to 6.1 ps/channel and analyzed globally with a time-resolved fluorescence analysis (TRFA) software. The full width at half-maximum (FWHM) of the IRF was typically in the order of 32 ps. The quality of the fits was judged by the fit parameters χ^2 (< 1.2), $Z\chi^2$ (< 3) and the Durbin Watson parameter (1.8<DW<2.2) as well as by the visual inspection of the residuals and autocorrelation function.[16] The fluorescent decays were analyzed first individually in terms of decay times and their associated pre-exponential factors.

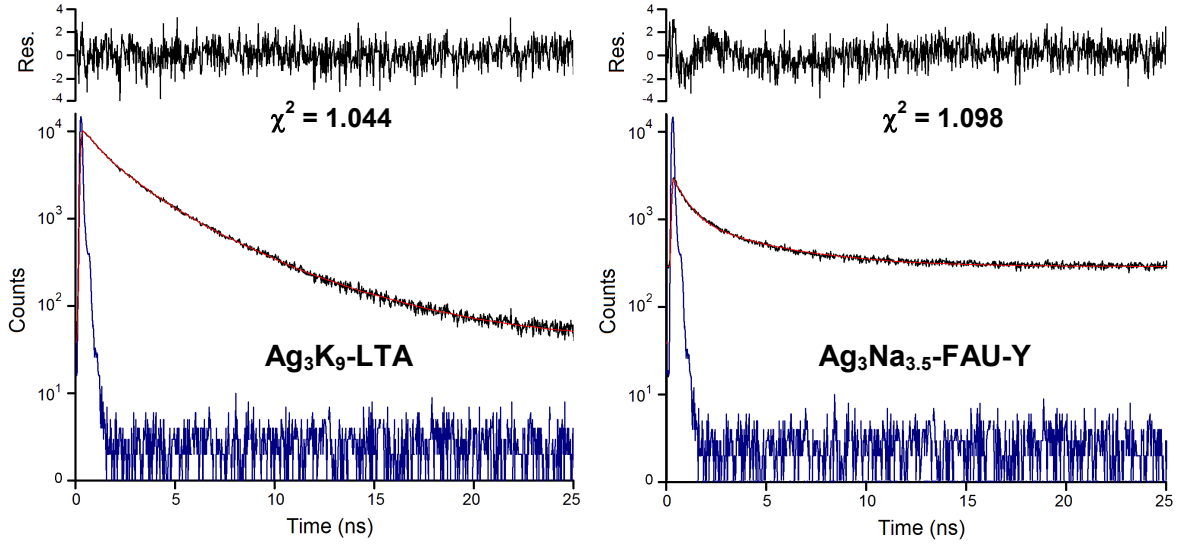

Figure S11. Fluorescence decay curves and fittings of Ag_3K_9-LTA and $Ag_3Na_{3.5}$-FAU-Y. Excitation 375 nm, detection 540 nm. The same analysis was performed for the rest of the samples.

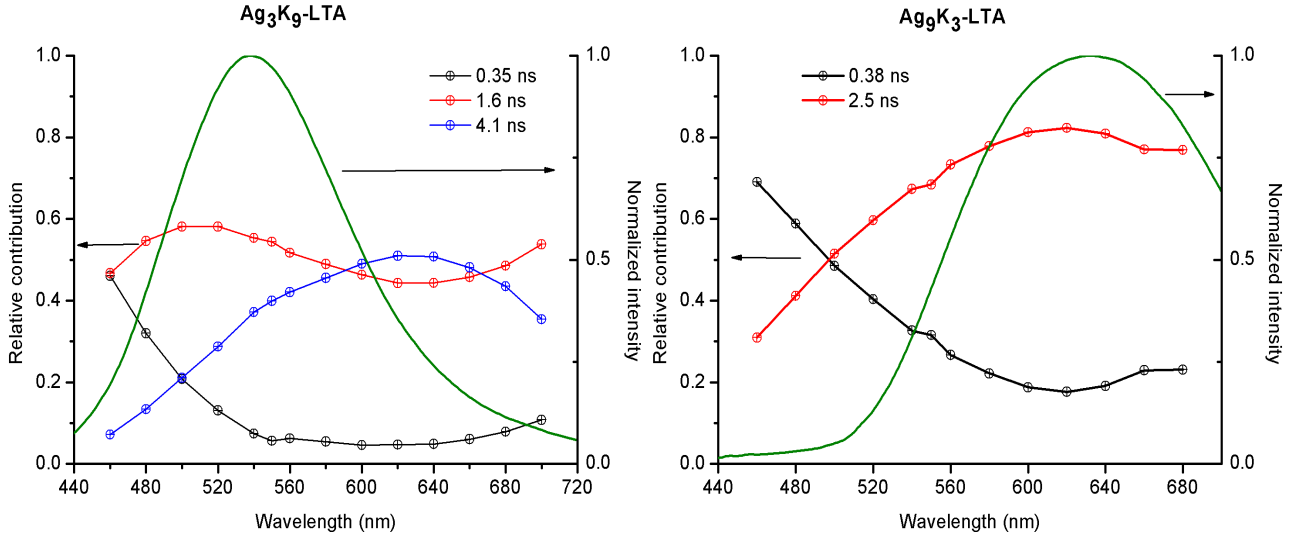

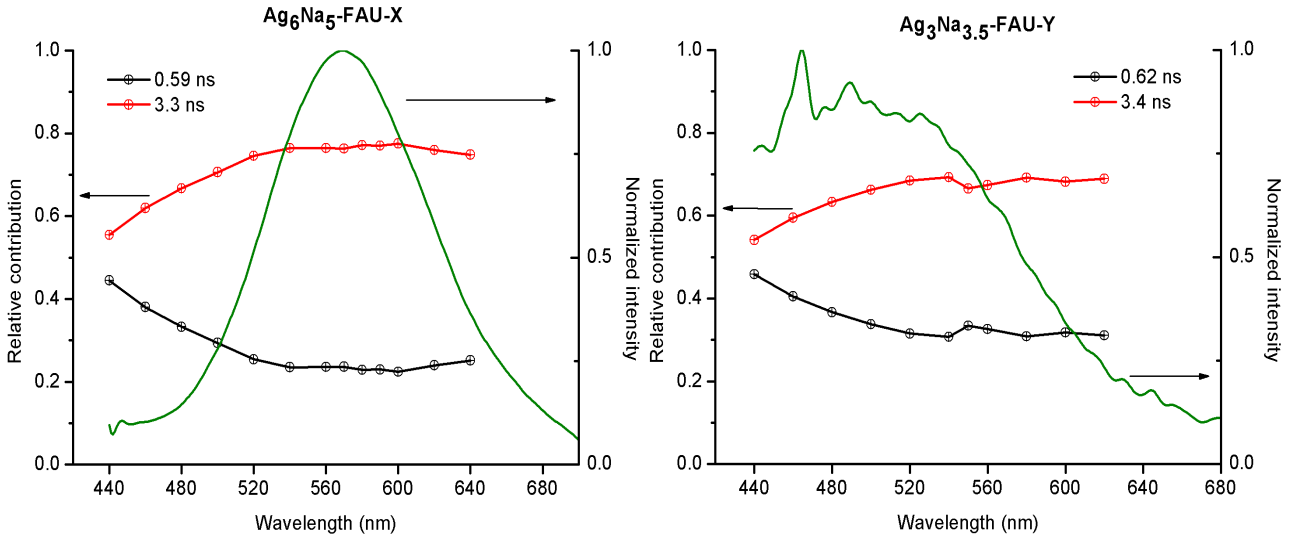

Figure S12. Relative contributions of the decay components as a function of emission wavelength for Ag_3K_9-LTA, Ag_9K_3-LTA, Ag_6Na_5-FAU-X, and $Ag_3Na_{3.5}$-FAU-Y. The emission spectra (375 nm excitation) of the X-ray activated samples is also shown (green line).

References

(1) G. De Cremer, E. Coutino-Gonzalez, M.B.J. Roeffaers, B. Moens, J. Ollevier, M. Van der Auweraer, R. Schoonheydt, P.A. Jacobs, F.C. De Schryver, J. Hofkens, D.E. De Vos, B.F. Sels and T. Vosch, *J. Am. Chem. Soc.,* 2009, **131**, 3049-3056.

(2) T. Sun and K. Seff, *Chem. Rev.* 1994, **94**, 857.

(3) J. Michalik and L. Kevan, *J. Am. Chem. Soc.* 1986, **108**, 4247.

(4) P.A. Jacobs, J.B. Uytterhoeven and H.K. Beyer, *J. Chem. Soc.* 1977, 128.

(5) R. Grosse, R. Burmeister, B. Boddenberg, Gedeon, A.; J. Fraissard, *J. Phys. Chem.* 1991, **95**, 2443.

(6) A. Mayoral, T. Carey, P.A. Anderson, A. Lubk and I. Diaz, *Angew. Chem. Int. Ed.* 2011, **50**, 11230-11233.

(7) E. Coutino-Gonzalez, M.B.J. Roeffaers, B. Dieu, G. De Cremer, S. Leyre, P. Hanselaer, W. Fyen, B. Sels and J. Hofkens, *J. Phys. Chem. C*, 2013, **117**, 6998-7004.

(8) Y. Sasaki and T. Suzuki, *Mater. Trans.* 2009, **50**, 1050-1053.

(9) R. Seifert, R. Rytz and G. Calzaferri, *J. Phys. Chem. A*, 2000, **104**, 7473-7483.

(10) C. Gauthier, V.A. Sole, R. Signorato, J. Goulon, and E. Moguiline, *J. Synchrot. Radiat.*, 1999, **6**, 164-166.

(11) P. Glatzel and U. Bergmann, *Coord. Chem. Rev.*, 2005, **249**, 65-95.

(12) F. M. F. de Groot, *Coord. Chem. Rev*. 2005, **249**, 31-63; O. V. Safonova, M. Tromp, J. A. van Bokhoven, F. M. F. de Groot, J. Evans, P. Glatzel, *J. Phys. Chem. B* 2006, **110**, 16162-16164; J. A. van Bokhoven, C. Louis. J. T. Miller, M. Tromp, O. V. Safonova, P. Glatzel, *Angew. Chem.* 2006, **118**, 4767-4770; *Angew. Chem. Int. Ed.* 2006, **45**, 4651-4654.

(13) D. E. Ramaker, D. C. Koningsberger, *Phys. Rev. Lett.* 2002, **89**, 139701; A. L. Ankudinov, J. J. Rehr, J. J. Low, S. R. Bare, *Phys. Rev. Lett.* 2002, **89**, 139702.

(14) T. Miyamoto, H. Niimi, Y. Kitajima, T. Naito and K. Asakura, *J. Phys. Chem. A*, 2010, **114**, 4093-4098.

(15) G. De Cremer, Y. Antoku, M.B.J. Roeffaers, M. Sliwa, J. Van Noyen, S. Smout, J. Hofkens, D.E. De Vos, B.F. Sels and T. Vosch, *Angew. Chem. Int. Ed.*, 2008, **47**, 2813-2816.

(16) M. Maus, M. Cotlet, J. Hofkens, T. Gensch, F.C. De Schryver, J. Schaffer and C.A.M. Seidel, *Anal. Chem.* 2001, **73**, 2078-2086.